KSCE Journal of Civil Engineering (2023) 27(7):2766-2777
DOI 10.1007/s12205-023-0498-x

pISSN 1226-7988, eISSN 1976-3808
www.springer.com/12205

Geotechnical Engineering

Experimental Studies on Shear Behavior of Sand-Suction Caisson Wall Interface under Variable Normal Load and Penetration Rate

Yifan Li[a,b], **Dayong Li**[c], **Yuqi Wu**[c], **and Yukun Zhang**[a]

[a]*College of Civil Engineering and Architecture, Shandong University of Science and Technology, Qingdao 266590, China*
[b]*School of Architecture and Engineering, Weifang University, Weifang 261041, China*
[c]*College of Pipeline and Civil Engineering, China University of Petroleum (East China), Qingdao, Shandong 266580, China*

ARTICLE HISTORY

Received 29 March 2022
Revised 7 July 2022
Accepted 13 April 2023
Published Online 29 May 2023

KEYWORDS

Suction caissons
Interface shear behavior
Variable normal load
Shearing rate
Friction coefficient

ABSTRACT

Shear characteristics of the interface between sand and the suction caisson wall play an important role in determining the friction resistance along the suction caisson wall. In this study, a variable normal load (VNL) reflecting the effects of the penetration depth and installation rate of a suction caisson is applied using the torsional interface shear apparatus to examine the interface shear behavior. Results show that the interface friction coefficient decreases with the increase of the normal stress and shearing rate until reaching a critical value. When the friction coefficient reaches the critical value, the friction coefficient changes little with the increase of normal stress. The variation of the friction coefficient caused by the seepage flow and penetration rate should be considered for calculating the frictional force along the caisson wall. Given the same shearing rate, the normalized efficiency parameter of the interface under the VNL is higher than that obtained under the CNL. The suction calculated based on the test results of this study is in good agreement with that from the Tenby project, indicating that our findings are reliable and beneficial to analyze the installation process of the suction caisson.

1. Introduction

Suction caissons are gaining significant attention as foundation solutions to numerous offshore applications, such as fixing platforms and supporting offshore wind turbines (Pérez-collazo et al., 2015; Wu et al., 2019). The suction that results from the inside water pressure being lower than the outside water pressure induces seepage flow into the caisson during installation in a sandy seabed (Oh et al., 2018; Ragni et al., 2020). The seepage causes a change in radial pressures on the inner and outer sides of the caisson wall. The relationships between the penetration resistance, required suction, and other factors can be determined by analyzing the mechanical behavior of the sand–suction caisson wall interface.

The mechanical properties of the interface are critical for studying the soil–structure interaction (Burgess, 1983; Uesugi and Kishida, 1986; Hu and Pu, 2004). Many researchers have conducted experimental studies on the mechanical characteristics of the soil–structure interface. It has been shown that several factors affect the shearing response of interfaces, including the soil properties (Canakci et al., 2016; Feligha et al., 2016), particle morphology and gradation (Fuggle, 2011; Vangla and Latha, 2016; Rui et al., 2021), confinement conditions (Dietz and Lings, 2006; Farhadi and Lashkari, 2017), surface structure characteristics (Taha and Fall, 2013; Martinez and Frost, 2017), and soil moisture content (Borana et al., 2016; Al-Emami, 2018). The penetration depth and rate are important factors affecting the lateral friction resistance when installing the suction caisson. Therefore, this study aims to investigate the effect of confinement conditions and shearing rates on the interface shear strength during installation of the suction caisson.

Generally, there are three normal confinement conditions in shear tests: 1) constant normal load (CNL) conditions, 2) constant normal displacement (CND) conditions, and 3) constant normal stiffness (CNS) conditions. Ghionna and Mortara (2002) found that the differences observed between the interface friction angles derived from model pile tests and the interface direct shear tests performed at CNL are due to the tendency of the interface soil to

CORRESPONDENCE Dayong Li ldy@upc.edu.cn College of Pipeline and Civil Engineering, China University of Petroleum (East China), Qingdao, Shandong 266580, China

dilate or contract in a restraining medium, whereas a CNS direct shear apparatus could prevent this issue. Nardelli et al. (2019) performed direct shear tests on the sand–concrete interface to investigate the effects of the surface roughness, mean sand diameter, and relative density on the interface strength and behavior under different confinement conditions. It was found that the CNS conditions correspond to the soil–structure interface in deep foundations. The differences between the test results under two different conditions were also analyzed. In order to study the influence of the bolt inclination angle and boundary conditions on the shear behavior and failure characteristics of bolted joints, direct shear tests under both CNL and CNS conditions were conducted by Cui et al. (2020). It was demonstrated that the shear strength is underestimated under CNL conditions, whereas dilation is overestimated, indicating that the normal stiffness cannot be neglected in engineering applications. Therefore, normal confinement conditions should be considered in the interface shear tests for practical applications. The interface shear tests under CNL conditions can be used for the case in which the structure is subjected to a static load, and the relative displacement is small; similar situations include shallow foundations, retaining walls, embankments, geotextiles, and anchoring systems. When the soil–structure interface undergoes large relative displacements and the normal stress is constantly changing (such as during the penetration of jacked piles and suction caissons), the interface shear test under CNS conditions or variable normal stress conditions can better reflect the actual interface mechanical properties.

The shearing rate is also an essential factor affecting the shear behavior of the soil–structure interface. Several researchers have carried out investigations on the shearing rate. El-Mhaidib (2006) conducted direct shear tests to investigate the effect of the shearing rate on the interface friction angle between sand and steel. It was shown that both the internal friction angle of sand and the interface friction angle increase with the increase in the shearing rate. Ganesan et al. (2014) carried out a series of interface direct shear tests on marine clay and found that the peak value of the interface friction is influenced by the pre-consolidation pressure, shearing rate, and interface roughness. The rate at which the peak strength reduced was found to strongly depend on the shearing rate and the interface roughness. Boukpeti and White (2017) investigated the shearing rate effects on soil–pipeline interfaces at low effective stresses by conducting direct shear tests and concluded that the drainage state could be controlled by the shearing rate. The results also confirmed that the interface residual stress ratio decreased with increasing shearing rate. Martinez and Stutz (2019) revealed the influence of the shearing rate on the shear behavior of the clay–steel interface through direct shear tests. It was shown that increasing the shearing rate resulted in an excessive pore–water pressure, which led to a decrease in the interface strength. Sweta and Hussaini (2019) evaluated the shear behavior of unreinforced and geogrid-reinforced ballast–sub–ballast interfaces at different shearing rates. The test results indicated that the friction and shear expansion angles at the interfaces reduced with the increase in the shearing rate, while the breakage of the ballast increased.

Many previous studies conducted interface shear tests with the aim of analyzing the factors affecting the interface shear behavior under CNL and CNS conditions, and the samples used were rarely saturated. There are no experimental studies that specifically address the suction caisson–soil interface. However, a large displacement occurs at the sand–suction caisson wall interface during installation of the suction caisson in saturated sand, and the seepage induced by suction causes radial pressure changes on the inner and outer sides of the caisson wall. In this work, the effects of the penetration rate and depth on the shear behavior of the sand–suction caisson wall interface in saturated fine sand were studied using a large displacement interface shear apparatus. Four different penetration rates were set with reference to the field installation of several projects. In order to simulate the penetration of the suction caisson, a variable normal load (VNL) was used to analyze the shear behavior of the sand–suction caisson wall interface at different penetration depths and explore the shear strength parameters. This work aims to provide a new method for calculating the penetration resistance in terms of the interface shear strength of the sand–suction caisson wall for the first time.

2. Interface Shear Tests at Large Displacement

2.1 Experimental Setup

A series of laboratory tests were conducted using a torsional interface shear tester (IST) manufactured by GDS, UK (Fig. 1(a)). The GDS IST uses a continuous rotation, thereby providing an alternative option to a multiple reversal interface shear test. This system is capable of applying a continuous shear in one direction and maintaining the shear area unchanged. A linear or jumping torque, an axial pressure, and a shearing rate can all be implemented to simulate the variable load on suction caissons during penetration and service. The GDS IST applies an axial pressure through the axial pressing rod. The axial pressure rod and the suction caisson

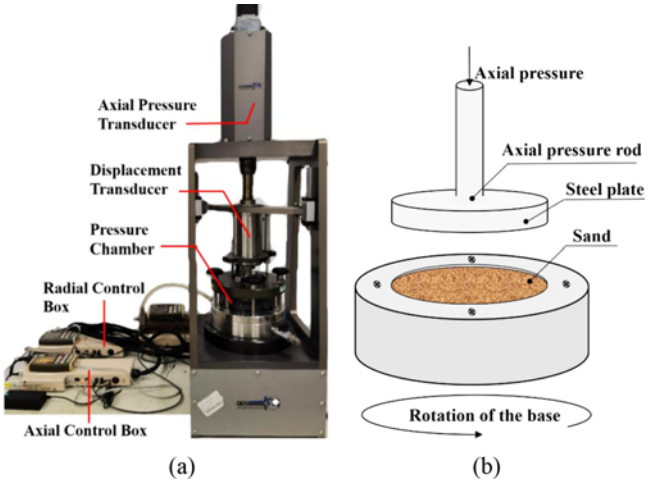

Fig. 1. GDS IST and Interface Shearing Illustration: (a) GDS IST, (b) Interface Shearing Illustration

are made of smooth steel, the effect of roughness is not considered. The bottom diameter of the pressure rod is 68 mm, and the height is 128 mm, as shown in Fig. 1(b). The influence of the curvature on the mechanical properties of the interface between the suction caisson and soil is not considered during the test. The bottom surface of the pressure rod simulates the suction caisson wall and forms an interface system with the soil inside the cutting ring. The shear is obtained through the rotation of the base. The continuously rotating platform can achieve a sufficiently large shear displacement for large deformation analysis, so the GDS IST has great advantages for studying the mechanical properties of the interface between the suction caisson and soil.

The diameter of the cutting ring is 70 mm, the height is 22 mm, and the shear area is 38.48 cm^2. The applied torsional force and the axial pressure are controlled by precision motors. The axial pressure and the torsional force can reach 5 kN and 200 N·m, respectively. The test process is controlled using a precision motor, and the test time, torsion force, axial force, axial deformation, and other test data are automatically recorded.

2.2 Experimental Materials

Quartz sand (QS) was collected from the Yellow Sea area of Qingdao in East China, as shown in Fig. 2. Figs. 2(a) and 2(b) shows the photographs of quartz sand particles obtained using a Carl Zeiss Stemi 2000–C microscope (Carl Zeiss Company, Germany) at 6.3 times and 50 times magnification, respectively. The distribution curve of the particle size and the basic physical properties of quartz sand are provided in Fig. 3 and Table 1, respectively.

2.3 Experimental Parameters

The penetration rate used in the test refers to the installation data of several projects in previously published article (Yuan et al., 2010). The average penetration rates of 0.2, 0.55, and 1.2 cm/min were obtained from the installation data of the suction caissons of the Tianjin Port North Breakwater Project, Europipe16/11-E platform, and Dagang Oilfield, respectively. Therefore, the shearing rates were set as 0.2, 0.5, 1.0, and 1.2 cm/min to investigate the influence of the penetration rate on the interface shear characteristics.

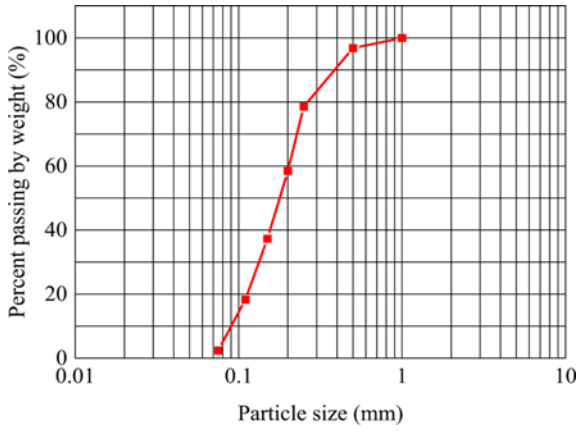

Fig. 3. Particle Size Distribution Curve of QS

Table 1. Basic Physical Properties of the Test Sand

Sand type	C_u	C_c	D_{50} (mm)	e_{max}	e_{min}	G_s
QS	2.13	0.48	0.18	0.7	0.8	2.49

Note: C_u = uniformity coefficient, $C_u = D_{60}/D_{10}$=2.13; C_c = coefficient of gradation, $C_c = D_{30}^2/D_{60}D_{10} = 0.48$; D_{50} = mean particle size; e_{max} = maximum void ratio; e_{min} = minimum void ratio; G_s = specific gravity of soil solids.

The penetration rate was converted into the required angular velocity using Eq. (1).

$$d = vt = (\pi/180)\omega rt, \tag{1}$$

where d is the shear displacement, $r = \int_0^R 2\pi r^2 dr/(\pi R^2) = (2/3)R$ is the mean radius (R = 34 mm is the radius of the bottom surface of the axial pressing rod), v is the penetration rate (cm/min), ω is the angular velocity (rad/min), and t is the shear time.

In order to accurately control the initial relative density of the sand samples and reduce the test errors, the relationship between the sand weight and the relative density was derived according to the basic physical parameters of sand. The maximum and minimum void ratios are commonly obtained by using the maximum and minimum densities. The initial relative density of the sand sample in the interface shear test was taken as 0.9, and the weight of the

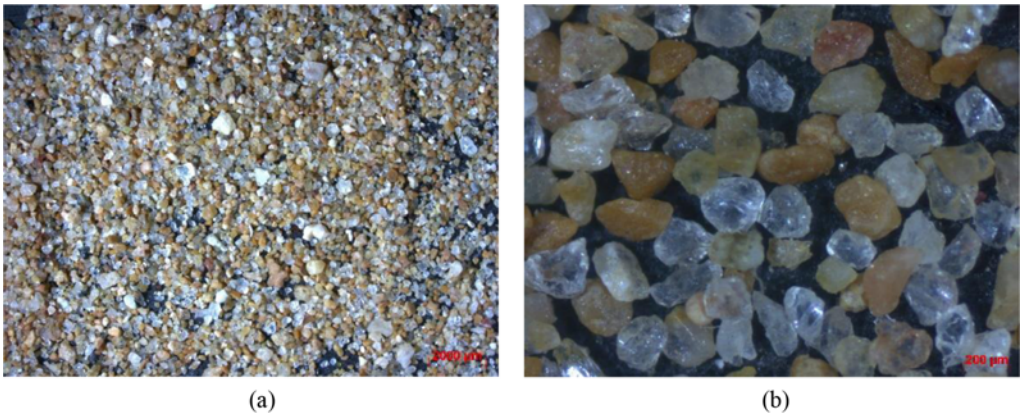

Fig. 2. Microscopic Images of Quartz Sand Particles: (a) 6.3 Times Magnification, (b) 50 Times Magnification

sand sample was calculated as 129.18 g.

2.4 Experimental Procedure

The rotating chassis was installed on the shearing platform, and the permeable stone, filter paper, cutting ring, and sealing ring were placed in sequence. The sand was added to the ring in three equal layers. The sand surface was smoothed and compacted using a rubber stick to make the sample reach the specified initial relative density. The pressure chamber was then installed, and distilled water was injected into the pressure chamber through the siphon method. The sample assembly process is shown in Fig. 4. The sand sample was left to saturate in the pressure chamber. After saturation, the shear test was performed. The sand sample parameters, shearing rate, and normal stress were set in the GDSLab software.

The experiments were performed to evaluate the relative influence of the penetration rate and depth on the shear behavior of the saturated fine sand–suction caisson interface during penetration. Four different shearing rates were set. In order to compare the test results with those under VNL conditions, interface shear tests at different shearing rates under CNL were conducted simultaneously, as shown in Table 2. The normal pressure was gradually increased from 0 kPa to the specified pressures of 10, 50, 100, or 200 kPa. The GDS IST was rotated clockwise for one cycle with a shear displacement of 144 mm.

After analyzing and comparing several suction foundation application projects (Yuan et al., 2010), the sand soil condition of the Tenby project (Houlsby and Byrne, 2005) was found to be the most similar to that of the sand used in this test; this can

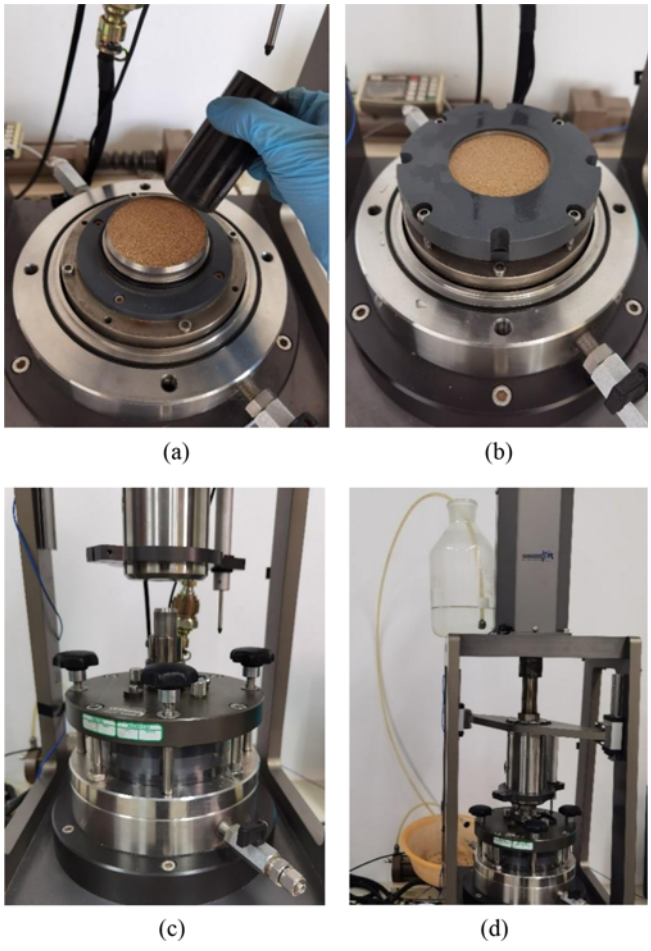

Fig. 4. Saturated Sample Installation Process: (a) Filling and Smoothing in Layers, (b) Sand Sample Assembly Completed, (c) Installing Pressure Chamber, (d) Injecting Distilled Water

Table 2. Summary of the Interface Torsional Shear Tests Conducted on the Saturated Interfaces

Interface state	Normal pressure (kPa)	Shearing rate (cm/min)
Saturated fine sand–steel	0 – 10, 10 0 – 50, 50 0 – 100, 100 0 – 200, 200	0.2; 0.5; 1.0; 1.2

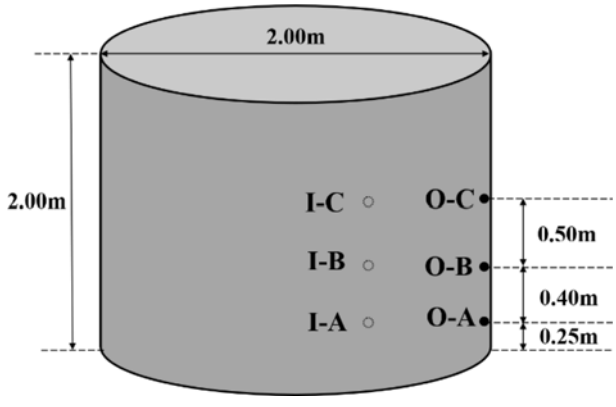

Fig. 5. Diagram of the Suction Caisson Reference Points

Table 3. Summary of the Interface Shear Tests Conducted on the Saturated Interfaces

Reference point	(Penetration at 0.5 m) Radial pressure (kPa)	(Penetration at 1 m) Radial pressure (kPa)	(Penetration at 1.4 m) Radial pressure (kPa)	(Penetration) Shearing displacement (m)	Penetration rate (cm/min)
O-A (outer wall)	15.1	34.5	53.7	1.15	1.0
I-A (inner wall)	3.5	2.8	2.2	1.15	
O-B (outer wall)	0	17.2	35.8	0.75	
I-B (inner wall)	0	1.3	1.46	0.75	
O-C (outer wall)	0	0	17.9	0.25	
I-C (inner wall)	0	0	0.7	0.25	

reduce the experimental error. In order to mimic the mechanical characteristics of the sand–caisson interface during the penetration of the caisson under suction in engineering, the actual working condition was simulated based on the Tenby engineering data. The positions of 0.25, 0.65, and 1.15 m upward from the bottom of the caisson were used as reference points A, B, and C (Fig. 5). Table 3 summarizes the changes in the soil pressure on the inner and outer sides of the caisson wall and the displacements during penetration of points A, B, and C during the process of applying suction. The soil pressure and the penetration displacement of the inner and outer walls of the three reference points were set as the axial pressure and the shear displacement of the GDS IST so that the mechanical properties of the interface between the saturated fine sand and the suction caissons under the actual shear path could be explored.

3. Test Results

3.1 Interface Normal Displacement–Shear Displacement Curves under VNL

Figure 6 shows the interface normal displacement–shear displacement curves of saturated fine sand–suction caisson at different penetration rates. In the interface shear test, the interface shear area remained constant, and the volume change of soil sample could be expressed by the normal displacement. In this paper, the value of sample compression is negative and the sample volume decreases. With the increase of shear displacement, the normal displacement of saturated fine sand–suction caisson interface gradually decreases, the compression gradually increases, and the interface shear shrinkage phenomenon occurs. Under the same normal pressure, the normal displacement of the interface decreases and the interface compression increases with the decrease of penetration rate. When the normal pressure increases from 0 to 10 and 50 kPa, the normal displacement of the interface decreases slowly and varies from 0 mm to 0.4 mm. When the normal pressure increases from 0 to 100 and 200 kPa, the normal displacement of the interface decreases relatively quickly and varies from 0 mm to 0.64 mm.

3.2 Particle Gradation Change

Figure 7(a) shows the change of particle gradations before and after the shear of saturated fine sand–suction caisson interface at different penetration rates when the normal stress increases from 0 to 100 kPa. With the decrease of the penetration rate, under the

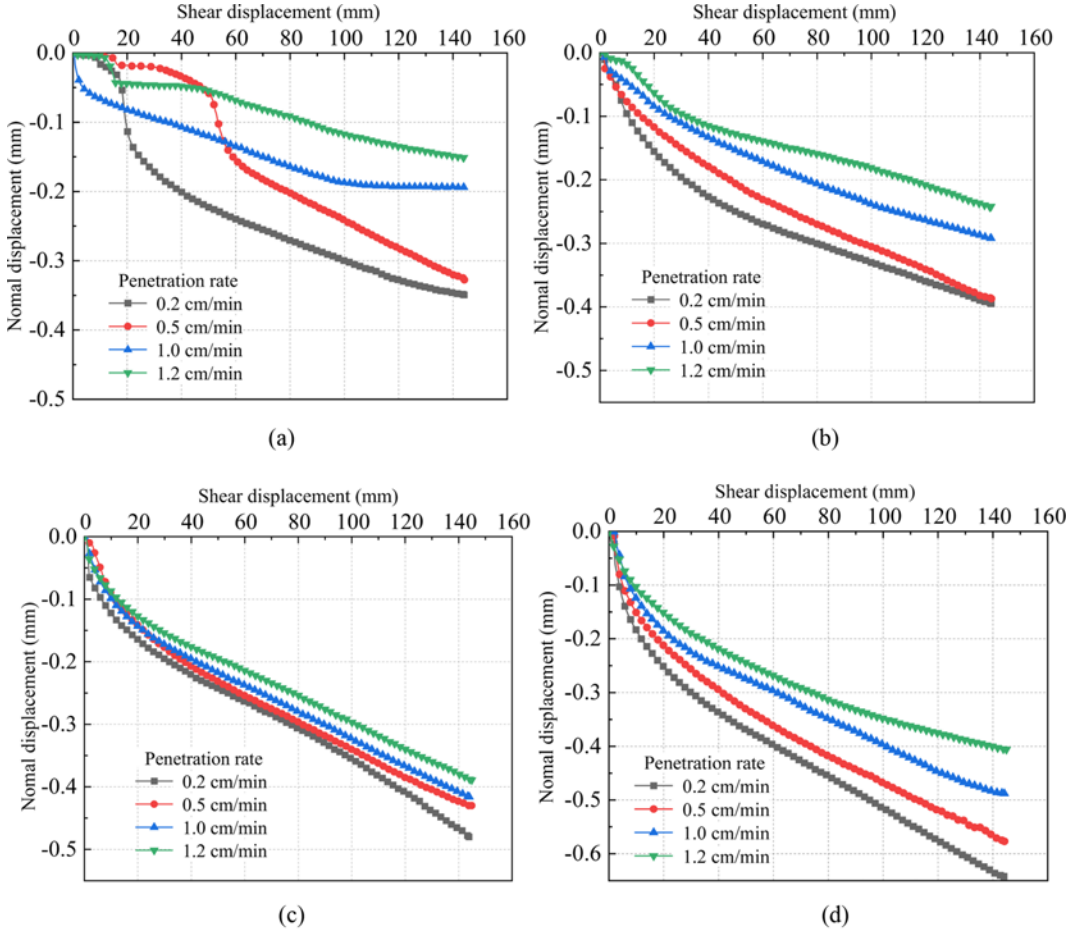

Fig. 6. Normal Displacement–Shear Displacement Curves of Saturated Fine Sand–Suction Caisson Interface at Different Penetration Rates: (a) 0 – 10 kPa, (b) 0 – 50 kPa, (c) 0 – 100 kPa, (d) 0 – 200 kPa

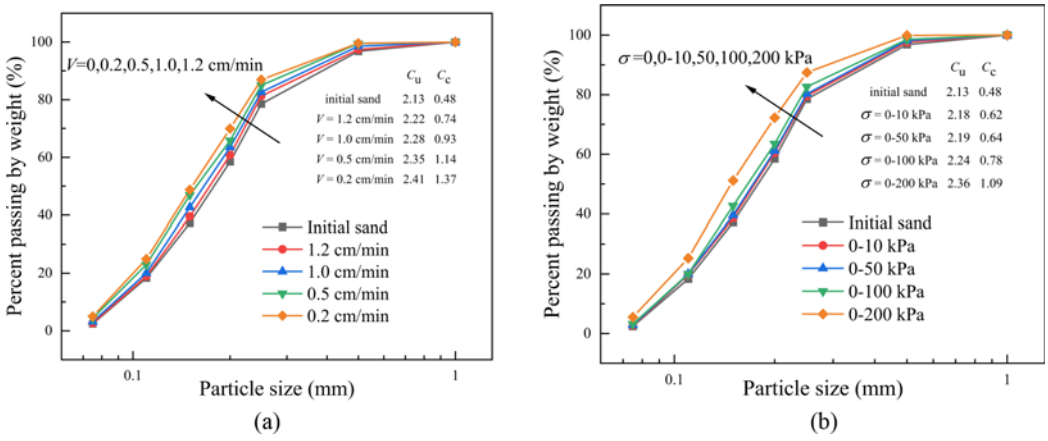

Fig. 7. Particle Gradations before and after 144 mm Shear Displacement under VNL: (a) With Different Penetration Rate under 0 – 100 kPa Normal Stress, (b) With Different Normal Stress at 1.0 cm/min Penetration Rate

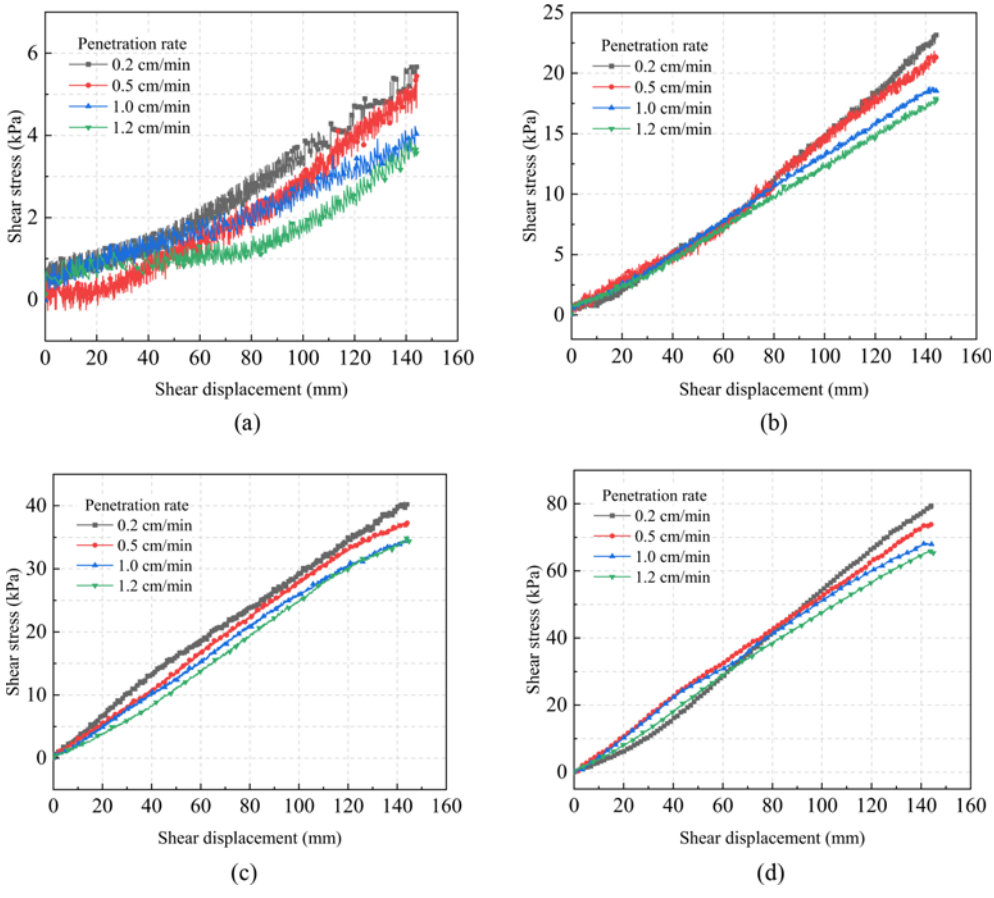

Fig. 8. Shear Stress–Shear Displacement Curves of the Saturated Fine Sand–Suction Caisson Interface at Different Penetration Rates: (a) 0 – 10 kPa, (b) 0 – 50 kPa, (c) 0 – 100 kPa, (d) 0 – 200 kPa

same shear displacement, the time becomes longer than that at the higher rate, and the large particle size is broken, leading to a gradual increase in the proportion of fine particles. Fig. 7(b) shows the change of particle gradations distribution before and after the shear of saturated fine sand–suction caisson interface under different normal stress conditions when the penetration rate is 1.0 cm/min. With the increase of normal stress, the proportion of fine particles increases gradually, and the particle breakage is obvious when the normal pressure increases from 0 to 200 kPa.

3.3 Interface Shear Stress–Displacement Curves under VNL

The observed trends of the saturated fine sand–suction caisson interface response under different penetration rates are plotted in Fig. 8. The curves of the shear stress–shear displacement for the

interface at different penetration rates show similar trends. With the continuous increase in the normal stress during the shear process, the shear stress increases with the shear displacement. The shear strength at the saturated fine sand–suction caisson interface decreases as the penetration rate increases. For example, when the normal stress increases from 0 to 100 kPa, the maximum shear strengths corresponding to a change in the penetration rate from 0.2 to 1.2 cm/min are 40.2, 37.3, 34.8, 34.3 kPa, respectively, and the slopes of the curves are 0.47, 0.44, 0.41, and 0.40 respectively. This is maybe caused by the fact that the sand particles at the interface have more time to realign to resist the shear action and exhibit a higher shear strength at a lower shearing rate than at a larger shearing rate. At the same time, as the other side of the interface is steel, the pore water at the interface can only diffuse in the direction of the soil. The accumulation of the pore water pressure under a higher shearing rate will also reduce the interface shear strength. This is in agreement with the findings of Martinez and Stutz (2019). However, these results contradict the findings regarding the sand–steel interface reported by El-Mhaidib (2006) at different shearing rates in dry sand. This shows that there are significant differences in the shear characteristics between the saturated and unsaturated soil–structure interfaces. The shear stress appears a certain few negative shear strengths below 0 at the initial stage when the normal stress increases from 0 to a certain value. This is because the GDS apparatus produces a certain amplitude of torque oscillation in order to ensure the increase of axial pressure. The ratio of negative value to maximum value is 0.035. So the negative value has no effect on the test results.

Figure 9 shows the shear stress versus shear displacement curves of the saturated fine sand–suction caisson interface under VNL. As the normal stress increases, the interface shear stress increases significantly, indicating that the penetration depth has a pronounced effect on the shear stress at the interface. The normal stress gradually increases from 0 to each desired normal stress level. No strain softening will occur, and the peak shear strength of the interface cannot be obtained. The reason is that there are two different soil evolution behaviors near the interface, i.e., the increase in the sand relative density and the sand particle fragmentation. The normal stress increases continuously, which leads to a gradual increase in the relative density. At the same time, the shearing action causes the breakage of sand particles. The broken particles fill the pores to make the sand denser, which results in an increase in the contact area between the sand particles. The stronger the interlocking action between the sand particles, the more difficult it is for the particles to stagger and tumble each other, which results in a higher maximum shear strength at the interface. The above analysis conclusions can be

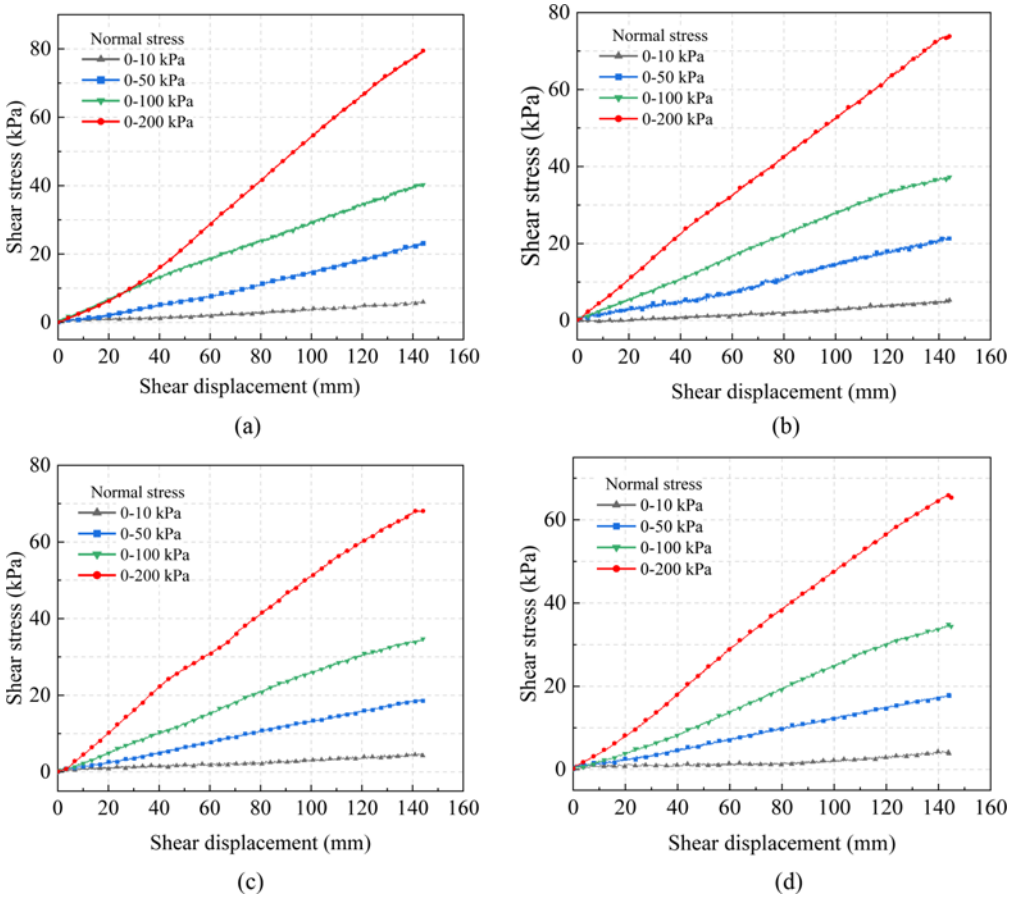

Fig. 9. Shear Stress–Displacement Curves of the Saturated Fine Sand-Suction Caisson Interface under VNL Conditions: (a) 0.2 cm/min, (b) 0.5 cm/min, (c) 1.0 cm/min, (d) 1.2 cm/min

Table 4. Results of the Torsional Interface Shear Tests and Sand Direct Shear Tests

Normal stress (kPa)	Penetration rate (cm/min)	τ_m/σ_{var}	τ_p/σ_{con}	δ_{mvar} (°)	δ_{pcon} (°)	φ_p (°)	E_{pVNL}	E_{pCNL}
	0.2	0.55	0.36	28.84	19.81	33.72	0.83	0.54
0 – 10	0.5	0.49	0.34	26.17	18.79	32.00	0.79	0.53
10	1.0	0.43	0.32	23.09	17.75	34.92	0.61	0.46
	1.2	0.41	0.28	22.51	15.65	36.22	0.57	0.38
	0.2	0.47	0.29	25.07	16.18	31.30	0.77	0.48
0 – 50	0.5	0.43	0.25	23.09	13.97	32.09	0.68	0.40
50	1.0	0.37	0.22	20.45	12.49	34.29	0.55	0.32
	1.2	0.36	0.20	19.56	11.32	36.90	0.49	0.28
	0.2	0.42	0.25	22.91	13.81	30.93	0.71	0.41
0 – 100	0.5	0.38	0.22	20.96	12.49	31.61	0.63	0.36
100	1.0	0.35	0.20	19.25	11.32	34.41	0.51	0.29
	1.2	0.34	0.19	18.95	10.53	37.24	0.45	0.24
	0.2	0.40	0.24	21.64	13.27	30.68	0.67	0.39
0 – 200	0.5	0.37	0.22	20.45	12.49	32.16	0.59	0.35
200	1.0	0.34	0.19	18.95	10.92	34.88	0.49	0.28
	1.2	0.33	0.18	18.34	10.13	35.61	0.46	0.25

Note: τ_m = Maximum interface shear stress under VNL conditions; τ_p = Interface shear strength under VNL conditions; σ_{var} = Normal stress increases from 0 to a specified value during interface shear; σ_{con} = Constant normal stress; δ_{mvar} = Maximum friction angle of the interface under VNL conditions; δ_{pcon} = Peak friction angle of the interface under CNL conditions; E_{pVNL} = normalized efficiency parameter under VNL conditions; E_{pcNL} = normalized efficiency parameter under CNL conditions (see section 3.3 for details).

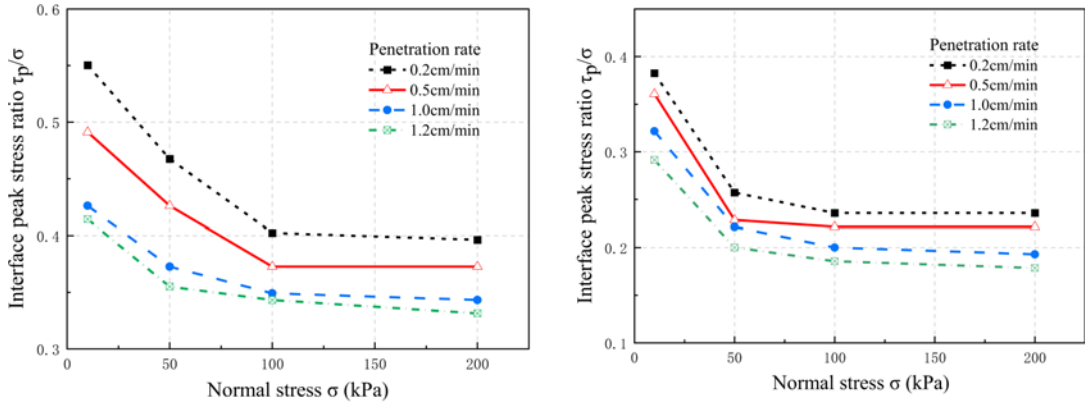

Fig. 10. Interface Friction Coefficient–Normal Stress Curves at Different Penetration Rates: (a) VNL Conditions, (b) CNL Conditions

confirmed by the normal displacement–shear displacement curves (Fig. 6) and the change of particle gradations before and after shear (Fig. 7).

3.4 Interface Friction Coefficient under VNL and CNL (τ/σ)

Table 4 provides all the interface shear test results and the corresponding normalized parameters. The peak friction angle φ_p of the sand was obtained using a ShearTrac-II strain-controlled direct shear apparatus at the normal stresses of 10, 50, 100, and 200 kPa according to the penetration list provided in Table 2.

To further investigate the effect of the penetration rate and the normal stress on the interface friction coefficient, the friction coefficient–normal stress (τ/σ–σ) curves under VNL and CNL conditions at different penetration rates are plotted in Fig. 10 according to the results presented in Table 4. The friction coefficient decreases with the increase in normal stress and shearing under VNL and CNL conditions. Fig. 10(a) shows the sharp decrease in the friction coefficient with increasing normal stress; it then stabilizes when the final value of the normal stress is less than 100 kPa, regardless of the penetration rate. It is observed that there is a critical value beyond which little change occurs. The critical value is 50 kPa under CNL conditions, as shown in Fig. 10(b). Under a higher normal stress, the pore water pressure at the interface dissipates more slowly. The maximum shear stress cannot raise significantly, which results in a constant friction coefficient.

3.5 Normalized Efficiency Parameter

Interface strengths are reported in terms of the normalized efficiency parameter E, which was defined by Koerner (1990) according to Eq. (2).

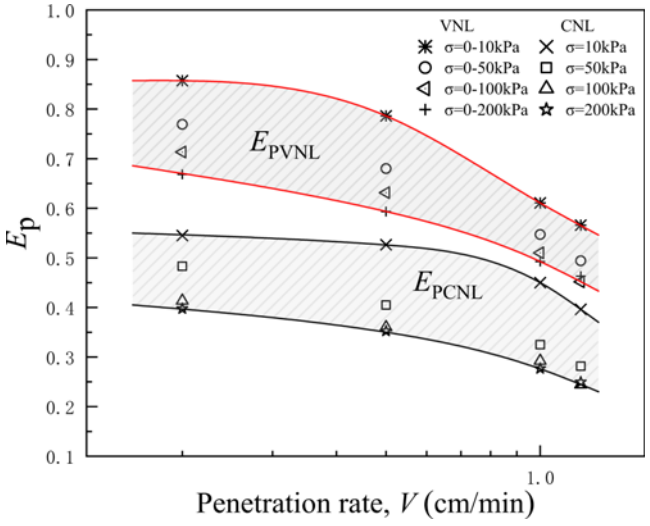

Fig. 11. Normalized Efficiency Parameter E_p-Penetration Rate V Curves

$$E = \frac{\tan\delta}{\tan\varphi_p}, \tag{2}$$

where $\tan\delta$ is the interface friction coefficient, and $\tan\varphi_p$ is the granular material friction coefficient. The maximum or peak efficiency parameter E_p can be computed via Eq. (2) using the appropriate values of the friction coefficients presented in Table 4. The efficiency parameter approaches nearly 0 if the interface strength is small. The efficiency parameter is equal to, or greater than 1.0 when the full soil strength is mobilized (Dove and Jarrett, 2002; Jin et al., 2018). In order to investigate the penetration rate effects on the frictional properties of the interface under variable normal stress and constant normal stress, the efficiency parameter E_p is plotted against the penetration rate in semilogarithmic coordinates in Fig. 11 based on the experimental data presented in Table 4. Fig. 11 provides a range for the efficiency parameter E_p as a function of the penetration rate V at the sand–suction caisson wall interface under VNL and CNL conditions.

Figure 11 shows that:1) The efficiency parameter decreases linearly with the increase in the logarithm of penetration rate V; 2) The effects of the penetration rate on the interface shear effectiveness under VNL and CNL conditions are almost the same, and the slopes are similar; 3) The overall effectiveness of the interface under VNL is higher than that under CNL under the conditions in this experiment. Since soil and steel are two materials with very different properties, their intermolecular adhesion is small. A water film exists between the saturated soil and steel. As the shearing rate increases, the unit contact time decreases. The interaction between the ends of the molecular chains covering the water film at the interface weakens, and the efficiency parameter E_p decreases.

3.6 Shearing Behavior of the Sand–Suction Caisson Wall Interface during the Tenby Suction Caisson Penetration

Large displacement interface shear tests were conducted, as presented in Table 3. The maximum shear displacement was up to 1,150 mm, and the penetration phase under a negative pressure applied to the suction caisson was simulated. Fig. 12 shows the shear stress–displacement curves on the inner and outer walls of the three reference points, namely A, B, and C, during the penetration of the suction caisson. Under a smaller radial pressure, the interface shear law of the reference points on the inner walls, namely I-A, I-B, and I-C, is consistent. The shear stress continuously varies around 1 kPa, which reflects the pronounced seepage drag reduction effect of the inner wall of the caisson during penetration of the suction caisson. The radial pressure on the outer wall of the caisson increases significantly during penetration of the suction caisson, and the shear stress increases gradually as the shear displacement increases to the maximum value without the strain-softening phenomenon. Fig. 13 shows the radial pressure at different reference points versus the penetration depth curves. The larger the increment of the radial pressure

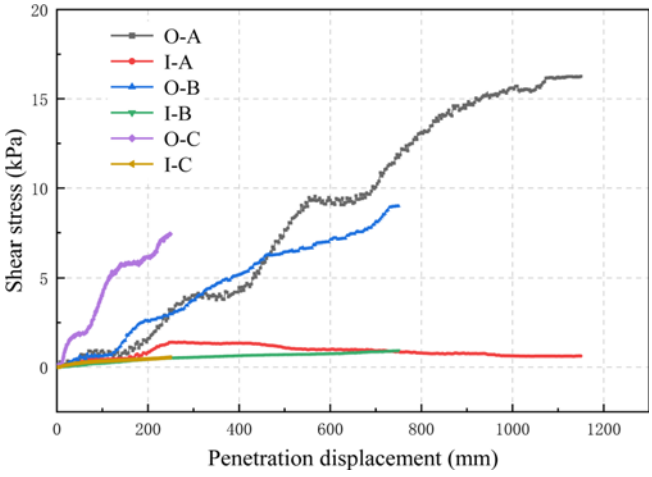

Fig. 12. Shear Stress–Displacement Curve at the Different Reference Points during Penetration of the Suction Caisson

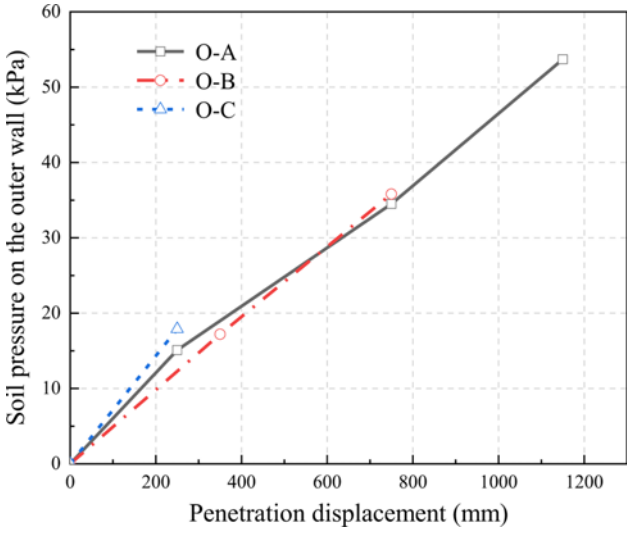

Fig. 13. Soil Pressure–Displacement Curve at the Different Reference Points on the Outer Wall

Table 5. Friction Coefficients of the Caisson–Soil Interface at Different Penetration Depths

Penetration depth (m)	Interface riction coefficient of the inner wall	Interface friction coefficient of the outer wall	Sum of the inner frictions (kPa)	Sum of the outer frictions (kPa)	Suction (kPa)
0.5	$\mu_{I\text{-}A} = 0.45$	$\mu_{O\text{-}A} = 0.48$	10.95	47.6	5.7
1.0	$\mu_{I\text{-}A} = 0.34$	$\mu_{O\text{-}A} = 0.38$	4.09	57.95	16.7
	$\mu_{I\text{-}B} = 0.33$	$\mu_{O\text{-}B} = 0.35$			
1.4	$\mu_{I\text{-}A} = 0.29$	$\mu_{O\text{-}A} = 0.28$	3.68	85.53	25.4
	$\mu_{I\text{-}B} = 0.27$	$\mu_{O\text{-}B} = 0.24$			
	$\mu_{I\text{-}C} = 0.33$	$\mu_{O\text{-}C} = 0.29$			

within unit displacement (i.e., the slope of the line) in Fig. 13 is, the faster the shear stress increases with the displacement in Fig. 12 will be. This is due to the fact that when the radial pressure increment is larger, more particles are crushed in a short time and the relative density of the sand increases. Therefore, the contact between the particles is large, and the higher energy of the interface particles driving other particles under shear shows a higher shear stress.

As shown in Fig. 12, the maximum interface friction coefficients of the inner and outer sides of the caisson wall at different penetration depths at points A, B, and C are summarized in Table 5. Combined with the soil pressure provided in Table 3, the internal and external friction resistance of the caisson wall can be obtained according to Eqs. (3), (4). The tip resistance of the suction caissons in saturated fine sand during suction-assisted penetration can be ignored (Senders and Randolph, 2009; Chen et al., 2016; Zhang et al., 2017; Liu et al., 2019). The required suction for different penetration depths can be obtained according to Eq. (5), as shown in Table 5.

$$R_{\mathrm{fI}} = \sum_{i=1}^{3} p'_{\mathrm{Ii}} \cdot \mu_{\mathrm{I}} \cdot A_{\mathrm{Ii}}, \tag{3}$$

$$R_{\mathrm{fO}} = \sum_{i=1}^{3} p'_{\mathrm{Oi}} \cdot \mu_{\mathrm{O}} \cdot A_{\mathrm{Oi}}, \tag{4}$$

$$0.25 \cdot \pi D_{\mathrm{i}}^2 \cdot s + V' = R_{\mathrm{fI}} = f_{\mathrm{fO}}, \tag{5}$$

where R_{fI} and R_{fO} are the inner and outer friction values of the caisson wall, μ is the interface friction coefficient, $A_{\mathrm{I}} = \pi D_{\mathrm{i}} h$ and $A_{\mathrm{O}} = \pi D_{\mathrm{o}} h$ are the areas of the caisson wall represented by the inner and outer reference points, respectively, D_{i} and D_{o} are the inner and outer diameters of the caisson, respectively, h = 0.45, 0.55, and 0.40 m from the bottom of the caisson, s is the suction, and V' is the caisson submerged self-weight. The values of V', D_{i}, and D_{o} were taken from a previous work (Houlsby and Byrne, 2005).

Figure 14 shows the comparison between the calculated results and the measured data. It can be seen that the observed suction against the penetration response can be well fitted, and the calculated suction is slightly higher than the measured suction. This is due to the fact that the tip resistance is ignored in the calculation, and only three reference points are selected. The accuracy of the frictional resistance calculation needs to be improved. However, the overall calculated suction pressure is in good agreement with the measured data, indicating that the measured interface friction coefficient is accurate.

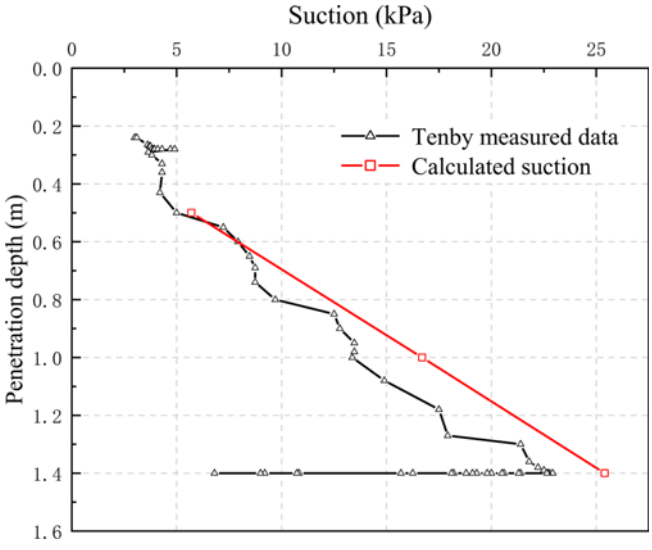

Fig. 14. Calculated Suction and Case Records for the Tenby Installation

4. Conclusions

This paper presented a series of torsional interface shear tests to study the interface shearing behavior between saturated fine sand and the suction caisson. The effects of the penetration depth and rate on the shear characteristics of the saturated fine sand–caisson interface were investigated. The main conclusions are as follows.

1. Two different soil evolution behaviors occur near the interface under VNL conditions, namely the increase in the density and the crushing of particles. Thus, the higher interface shear strength is reached as the normal stress increases without strain softening during shearing. The maximum interface shear stress increases as the penetration rate decreases due to the fact that the sand particles at the interface have more time to realign to resist the shear action.
2. The interface friction coefficient decreases with the increase in normal stress and shearing rate under VNL and CNL conditions. The interface friction coefficient under VNL conditions is higher than the case under CNL conditions, and there exists a critical value beyond which the interface

friction coefficient exhibits little change. The critical values are 100 and 50 kPa under VNL and CNL conditions, respectively. The variation in the friction coefficient caused by the seepage flow and the penetration rate should be considered when calculating the friction along the caisson wall in sand.

3. The efficiency parameter E_p decreases with the increase in the logarithm of the penetration rate V. The normalized efficiency parameter of the interface under VNL conditions is higher than the case under CNL conditions at the same penetration rate.
4. The interface test results under VNL conditions can better reflect the interface characteristics of suction caisson installations. Based on these results, the suction required for the caisson installation in the Tenby project was calculated and was well fitted by the observed suction against penetration response. The findings presented in this study can be a guidance for calculating the required suction for suction caisson installations.
5. In future works, we will continue to study the shear characteristics of saturated sand-suction caisson interfaces and establish mathematical models for interface strength, friction coefficient, and other relevant factors.

Acknowledgments

This study was financially supported by the National Science Foundation of China (Grant Nos. 51879044 and 51639002) and the SDUST Research Fund (Grant No. 2015KYJH104).

ORCID

Yifan Li https://orcid.org/0009-0006-3895-5285
Dayong Li https://orcid.org/0000-0001-7520-7071
Yuqi Wu https://orcid.org/0000-0002-8316-6182

References

Al-Emami O (2018) Investigation of soil-steel interface behavior of Iraqi soil by direct shear apparatus. *Matec Web of Conferences* 162: 01003, DOI: 10.1051/matecconf/201816201003

Borana L, Yin JH, Singh DN, Shukla SK (2016) Interface behavior from suction–controlled direct shear test on completely decomposed granitic soil and steel surfaces. *International Journal of Geomechanics* 16(6):D4016008, DOI: 10.1061/(ASCE)GM.1943-5622.0000658

Boukpeti, N, White DJ (2017) Interface shear box tests for assessing axial pipe–soil resistance. *Géotechnique* 67(1):18-30, DOI: 10.1680/jgeot.15.P.112

Burgess AS (1983) Elastic analysis of soil-foundation interaction. *Canadian Journal of Civil Engineering* 10(2):329, DOI: 10.1016/0013-7952(81)90027-2

Canakci H, Hamed M, Celik F, Sidik W, Eviz F (2016) Friction characteristics of organic soil with construction materials. *Soils Found* 56(6):965-972, DOI: 10.1016/j.sandf.2016.11.002

Chen F, Lian JJ, Wang HJ, Liu F, Wang HZ, Zhao Y (2016) Large-scale experimental investigation of the installation of suction caissons in silt sand. *Applied Ocean Research* 60:109-120, DOI: 10.1016/j.apor.2016.09.004

Cui GJ, Zhang CQ, Chen JL, Yang FJ, Zhou H, Lu JJ (2020) Effect of bolt inclination angle on shear behavior of bolted joints under CNL and CNS conditions. *Journal of Central South University* 27(3): 937-950, DOI: 10.1007/s11771-020-4342-x

Dietz MS, Lings ML (2006) Post peak strength of interfaces in a stress–dilatancy framework. *Journal of Geotechnical and Geoenvironmental Engineering* 132(11):1474-1484, DOI: 10.1061/(ASCE)1090-0241(2006)132:11(1474)

Dove JE, Jarrett JB (2002) Behavior of dilative sand interfaces in a geotribology framework. *Journal of Geotechnical and Geoenvironmental Engineering* 128(1):25-37, DOI: 10.1061/(ASCE)1090-0241(2002)128:1(25)

El-Mhaidib AI (2006) Influence of shearing rate on interfacial friction between sand and steel. *Engineering Journal of Qatar University* 19:1-16

Farhadi B, Lashkari A (2017) Influence of soil inherent anisotropy on behavior of crushed sand-steel interfaces. *Soils and Foundations* 57(1):111-125, DOI: 10.1016/j.sandf.2017.01.008

Feligha M, Hammoud F, Belachia M, Nouaouria MS (2016) Experimental investigation of frictional behavior between cohesive soils and solid materials using direct shear apparatus. *Geotechnical and Geological Engineering* 34(2): 567-578, DOI: 10.1007/s10706-015-9966-5

Fuggle AR (2011) Geomaterial gradation influences on interface shear behavior. PhD Thesis, School of Civil and Environmental Engineering, Georgia Institute of Technology, USA

Ganesan S, Kuo M, Bolton M (2014) Influences on pipeline interface friction measured in direct shear tests. *Geotechnical Testing Journal* 37(1):94-106, DOI: 10.1520/GTJ20130008

Ghionna VN, Mortara G (2002) An elastoplastic model for sand-structure interface behavior. *GeÂotechnique* 52(1):41-50, DOI: 10.1680/geot.52.1.41.40826

Houlsby GT, Byrne BW (2005) Design procedures for installation of suction caissons in sand. *Geotechnical Engineering* 158(3): 35-144, DOI: 10.1680/geng.158.3.135.66297

Hu LM, Pu JL (2004) Testing and modeling of soil-structure interface. *Journal of Geotechnical and Geoenvironmental Engineering* 130(8):851-860, DOI: 10.1061/(ASCE)1090-0241(2004)130:8(851)

Jin ZH, Yang Q, Chen C, Leng WM, Guo FQ, Zhao CY (2018) Experimental study on effects of the roughness on mechanical behaviors of concrete-sand interface. *Chinese Journal of Rock Mechanics and Engineering* 37(3):754-765, DOI: 10.13722/j.cnki.jrme.2017.1311 (in Chinese)

Koerner RM (1990) Designing with geosynthetics. Prentice Hall, Inc., Engelwood Cliffs, N.J. 652

Liu R, Ma WG, Qi Y, Wu XL (2019) Experimental studies on the drag reduction effect of bucket foundation installation under suction pressure in sand. *Ships and Offshore Structures* 14(5):421-431, DOI: 10.1080/17445302.2018.1500188

Martinez A, Frost JD (2017) The influence of surface roughness form on the strength of sand-structure interfaces. *Géotechnique Letters* 7:104-111, DOI: 10.1680/jgele.16.00169

Martinez A, Stutz HH (2019) Rate effects on the interface shear behavior of normally and overconsolidated clay. *Geotechnique* 69(9):801-815, DOI: 10.1680/jgeot.17.p.311

Nardelli A, Cacciari PP, Futai MM (2019) Sand-concrete interface response: The role of surface texture and confinement conditions. *Soils and Foundations* 59(6):1675-1694, DOI: 10.1016/j.sandf.2019.05.013

Oh KY, Nam W, Ryu MS, Kim JY, Epureanu BI (2018) A review of foundations of offshore wind energy convertors: Current status and future perspectives. *Renewable and Sustainable Energy Reviews* 88(C):16-36, DOI: 10.1016/j.rser.2018.02.005

Pérez-collazo C, Greaves D, Iglesias G (2015) A review of combined wave and offshore wind energy. *Renewable and Sustainable Energy Reviews* 42:141-153, DOI: 10.1016/j.rser.2014.09.032

Ragni R, Bienen B, O'Loughlin CD, Stanier SA, Morgan N (2020) Observations of the effects of a clay layer on suction bucket installation in sand. *Journal of Geotechnical and Geoenvironmental Engineering* 146(5):04020020, DOI: 10.1061/(ASCE)GT.1943-5606.0002217

Rui SJ, Wang LZH, Guo ZH, Chen XM, Wu B (2021) Monotonic behavior of interface shear between carbonate sands and steel. *Acta Geotechnica* 16:167-187, DOI: 10.1007/s11440-020-00987-9

Senders M, Randolph MF (2009) CPT-based method for the installation of suction caissons in sand. *Journal of Geotechnical and Geoenvironmental Engineering* 135(1):14-25, DOI: 10.1061/(ASCE)1090-0241(2009)135:1(14)

Sweta K, Hussaini SKK (2019) Behavior evaluation of geogrid-reinforced ballast-subballast interface under shear condition. *Geotextiles & Geomembranes* 47(1):23-31, DOI: 10.1016/j.geotexmem.2018.09.002

Taha A, Fall M (2013) Shear behavior of sensitive marine clay-concrete interfaces. *Journal of Geotechnical and Geoenvironmental Engineering* 139(4):644-650, DOI: 10.1061/(ASCE)GT.1943-5606.0000795

Uesugi M, Kishida H (1986) Influential factors of friction between steel and dry sands. *Soils Found* 26(2):33-46, DOI: 10.3208/sandf1972.26.2_33

Vangla P, Latha GM (2016) Effect of particle size of sand and surface asperities of reinforcement on their interface shear behavior. Geotext. *Geomembr* 44(3):254-268, DOI: 10.1016/j.geotexmem.2015.11.002

Wu XN, Hu Y, Li Y, Yang J, Duan L, Wang TG, Adcock T, Jiang ZhY, Gao Zh, Lin ZhL, Borthwick A, Liao ShJ (2019) Foundations of offshore wind turbines: A review. *Renewable and Sustainable Energy Reviews* 104:379-393, DOI: 10.1016/j.rser. 2019.01.012

Yuan ZL, Qin YL, Tang HY (2010) Shallow bucket foundation platform. Beijing: Petroleum Industry Press (in Chinese)

Zhang PY, Hu RQ, Ding HY, Guo YH, Xiong KP (2017) Comparative analysis of seepage field characteristics in bucket foundation with and without compartments. *Ocean Engineering* 143(1):34-49, DOI: 10.1016/j.oceaneng.2017.07.043